Hindawi Publishing Corporation
Mathematical Problems in Engineering
Volume 2014, Article ID 938618, 10 pages
http://dx.doi.org/10.1155/2014/938618

Research Article

Kinetic Study of Nonequilibrium Plasma-Assisted Methane Steam Reforming

Hongtao Zheng and Qian Liu

College of Power and Energy Engineering, Harbin Engineering University, Harbin 150001, China

Correspondence should be addressed to Hongtao Zheng; zhenghongtao9000@163.com

Received 29 November 2013; Accepted 9 September 2014; Published 28 September 2014

Academic Editor: Yonghong Wu

Copyright © 2014 H. Zheng and Q. Liu. This is an open access article distributed under the Creative Commons Attribution License, which permits unrestricted use, distribution, and reproduction in any medium, provided the original work is properly cited.

To develop a detailed reaction mechanism for plasma-assisted methane steam reforming, a comprehensive numerical and experimental study of effect laws on methane conversion and products yield is performed at different steam to methane molar ratio (S/C), residence time s, and reaction temperatures. A CHEMKIN-PRO software with sensitivity analysis module and path flux analysis module was used for simulations. A set of comparisons show that the developed reaction mechanism can accurately predict methane conversion and the trend of products yield in different operating conditions. Using the developed reaction mechanism in plasma-assisted kinetic model, the reaction path flux analysis was carried out. The result shows that CH_3 recombination is the limiting reaction for CO production and O is the critical species for CO production. Adding 40 wt.% Ni/SiO_2 in discharge region has significantly promoted the yield of H_2, CO, or CO_2 in dielectric packed bed (DPB) reactor. Plasma catalytic hybrid reforming experiment verifies the reaction path flux analysis tentatively.

1. Introduction

Chemically recuperated gas turbines (CRGT) are regarded as prospective advanced cycle engines due to high thermal efficiencies and low NO_x emissions. Steam reformer as the kernel component of CRGT can deeply recover turbine exhaust heat by fuel steam reforming. Traditional steam reforming process occurs in the conditions of high temperature (700–900°C) and high pressure (2-3 MPa). However, turbine exhaust temperature is only in the range of 350 to 500°C. Considering that plasma is a prospective tool without restriction from reaction temperature, nonequilibrium plasma-assisted fuel steam reforming technology for recycling exhaust heat in CRGT has been proposed. Because of the nonequilibrium characteristic of plasma, methane was converted into high hydrocarbons or synthesis gas in plasma-assisted steam reforming process. To seek the way to improve objective products yield, experimental and numerical researches on reforming process and reaction mechanism are necessary.

Recently, scholars researched plasma-assisted reforming mechanism by experiment and numerical simulation. In numerical researches, Rusu and Cormier [1] studied MSR in gliding arc reactor by thermodynamical equilibrium model; Petrovi et al. [2] studied the influence of gas flow rate and reactor geometry and applied voltage parameters on the discharge characteristics by fluid model but did not consider free radical reactions; Nair et al. [3] investigated plasma-assisted methane conversion in gas phase by partial oxidation at low energy density (80–200 kJ/mol CH_4) and low reactor temperatures (130–140°C) by constants substitution method; Li et al. [4] carried out kinetic simulation for methane coupled reaction based on Townsend ionization model; de Bie et al. [5] studied the conversion of methane to higher hydrocarbons or oxygenates by partial oxidation with CO_2 or O_2 in a dielectric barrier discharge by fluid model in Plasimo software. These researches mainly aimed at plasma-assisted methane coupling reactions, partial oxidation, and CO_2 reforming reactions and poorly referred to reaction mechanisms and kinetic effects for plasma-assisted methane steam reforming (MSR).

In experimental researches, there mainly existed two ways: one was to study the presence of dominating radicals by spectrograph [6, 7] and another was to conjecture some possible reaction pathways according to products [8–12].

However, they did not give out systematic reaction pathways for plasma-assisted reforming. What is more, recent studies of plasma-assisted MSR were carried out at water bath temperatures with low steam flow rates [10, 13]. So the study on plasma-assisted methane steam reforming in high flow rate of steam is very necessary.

In this paper, firstly, we study the effect laws of operating conditions on methane conversion and products yield to provide data support for reaction mechanism. Secondly, we develop a complete mechanism in order to estimate the real perspectives of MSR in plasma field and correct and hopefully perfect the mechanism further against sensitivity analysis module and experimental results. Thirdly, by employing the kinetic model and path flux analysis module, the kinetic effects of nonequilibrium plasma-assisted MSR on methane conversion are studied at 350–500°C without catalyst. At last, in order to preliminarily verify the validity of the reaction path flux analysis, plasma catalytic hybrid reforming experiment is employed.

2. Experimental Setup

Experimental setups are illustrated in Figure 1. The reactants were methane and steam; 10 vol% nitrogen was added to the methane cylinder as a reference for the quantitative analysis of the reformed gas after completion of the reaction. The flow rate of methane and nitrogen was controlled with mass flow controller (Brooks 5850E) and a tranquil flow pump was used to inject water (Beijing Xingda Co., 2PB00C). The feed gas flowed into DBD reactor after mixing. The DBD reactor employed quartz glass tube as dielectric and had a discharge gap of 1 mm and length of 130 mm and thus a total reactor volume of 12 cm^3, as seen in Figure 1(c). The reactor was heated by a ceramic heating pipe and the reaction temperature was controlled through the temperature controller. Due to thermal inertia, the measured values were deviated from the set point of about 5°C. The reactor was energized by an AC high discharge voltage 4 kV at a frequency of 41.93 kHz with a power equivalent of 70.13 W. To verify the running stability, the voltage and current values were recorded at the beginning and end of each experiment. The qualitative and quantitative analyses for products were conducted online using gas chromatography (Agilent GC 7890A). GC-FID (2 m DB-1 Column + 25 m HP-Al/S Column), GC-TCD B (Hayesep Q Column + Molecular Sieve 5 Å Column), and GC-TCD C (Hayesep Q Column + Molecular Sieve 5 Å Column) were used to determine the concentration of hydrocarbons, $CO/CO_2/N_2$, and H_2, respectively. Before flowing into gas chromatograph, the products were cooled by a cold trap and dried by allochroic silica gel. In order to ensure the accuracy of the measured data, the data were recorded after stabilizing the reforming system in any setting state for 20 min.

Experiments were carried out in different S/C, reaction temperatures, and residence time s with a pressure of 0.12 MPa. The standard conditions were a mass flow rate of 7.7×10^{-6} kg/s, reaction temperature of 400°C, plasma power, and frequencies of 70.13 W and 41.93 kHz, and S/C of 2. Experimental variations in different conditions are shown in Table 1, where three different mass flow rates are corresponding to residence time of 0.58, 0.39, and 0.29 s, respectively.

Table 1: Experimental variations in different conditions.

Effect factors	S/C	Reaction temperature/°C	Mass flow rate/(kg/s)
Variations	2, 3, 4, 5	350, 400, 450, 500	7.7×10^{-6}, 1.156×10^{-5}, 1.54×10^{-5}

3. Plasma-Reforming Kinetic Model

In order to further study gas-phase process and to have more insight into the chemical mechanism, a simple kinetic model has proven to be a useful technique. The numerical simulation was done with the assumption that radicals once produced were uniformly distributed within the whole volume, that is, a zero-dimensional model. The plasma-assisted steam reforming model incorporates a set of mass conservation and gas-phase species equations as well as electron energy equation. Based on the characteristic of plasma-assisted MSR, gas temperature T_g of the mixture was fixed in the set value. They were solved by CHEMKIN-PRO software [14]. The conservation equations are as follows:

global mass balance equation:

$$\frac{d}{dt}(\rho V) = \dot{m}^* - \dot{m} = 0, \tag{1}$$

species conservation equation:

$$(\rho V)\frac{dY_k}{dt} = \dot{m}^*(Y_k^* - Y_k) + \dot{\omega}_k V W_k, \tag{2}$$

state equation:

$$p = \sum_{k=1}^{K} \frac{\rho Y_k RT}{W_k}, \tag{3}$$

and electron energy equation:

$$\begin{aligned}
&(\rho V)\left[Y_e c_{ve}\frac{dT_e}{dt} - \frac{R}{W_e}T_e\frac{dY_e}{dt}\right] \\
&\quad = \dot{m}^* Y_e^* c_{pe}(T_e^* - T_e) - Q_{\text{loss}}^{\text{elas}} - Q_{\text{loss}}^{\text{inel}} + Q_{\text{source}}, \\
&Q_{\text{loss}}^{\text{elas}} = \frac{3VR\rho_e}{W_e}(T_e - T_g)\sum_{k=1,k\neq e}^{K_g}\frac{W_e}{W_k}\nu_{ek}, \\
&Q_{\text{loss}}^{\text{inel}} = V\sum_{r=1}^{I_{er}}\Delta H_r q_r.
\end{aligned} \tag{4}$$

Here $Q_{\text{loss}}^{\text{elas}}$ and $Q_{\text{loss}}^{\text{inel}}$ refer to the collision energy lost by the electrons both from elastic, momentum-transfer collisions and from inelastic collisional processes. The plasma-reactor model calculates the momentum-transfer collision

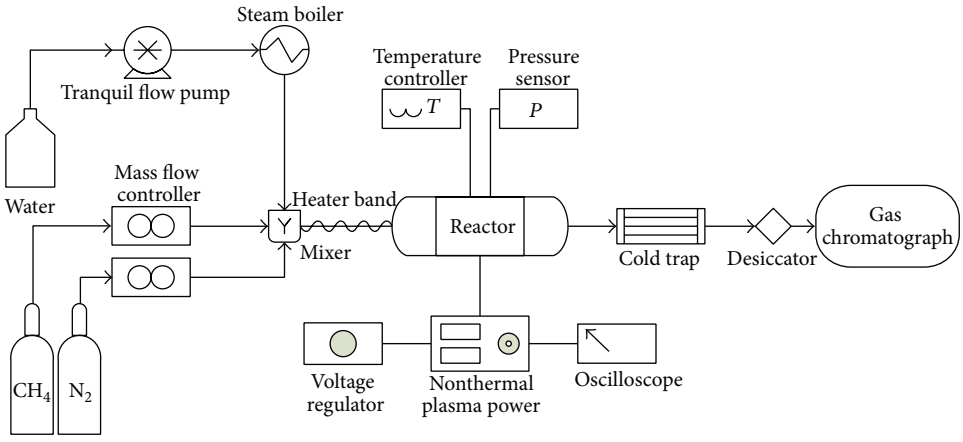

(a)

(b)

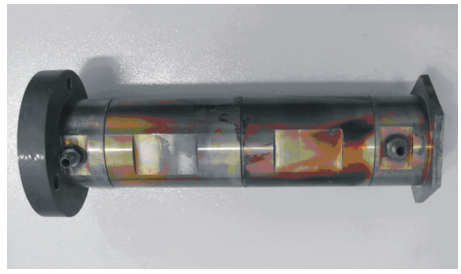

(c)

Figure 1: Experimental setup. (a) Schematic diagram of experimental setup, (b) photo of experimental equipment, and (c) photo of experimental reactor.

frequencies ν_{ek} from momentum-transfer collision cross-sections. $Q_{\text{loss}}^{\text{inel}}$ represents the summation of electron energy loss per electron-impact reactions. Q_{source} represents the power deposited through Joule heating into the plasma by acceleration of charged species along electric fields, namely, the effective input power. Consider the following:

chemical reaction progress equation:

$$q_r = k_{f,r}\prod_{k=1}^{K}[X_k]^{\upsilon'_{kr}} - k_{b,r}\prod_{k=1}^{K}[X_k]^{\upsilon''_{kr}}, \tag{5}$$

chemical reaction rate equation:

$$\dot{\omega}_k = \sum_{r=1}^{I_r}\left(\upsilon''_{kr} - \upsilon'_{kr}\right)q_r, \quad (k = 1, \ldots, K), \tag{6}$$

Arrhenius coefficients of electron-impact reactions:

$$k_{f,r,e} = A_r T_e^{\beta_r}\exp\left(-\frac{E_r}{RT_e}\right), \tag{7}$$

Arrhenius rate coefficients of free radical reactions:

$$k_{f,r,g} = A_r T_g^{\beta_r}\exp\left(-\frac{E_r}{RT_g}\right). \tag{8}$$

4. Results and Discussion

4.1. Experimental Process Analysis. In order to observe discharge phenomenon conveniently to confirm normal discharge and furthermore to determine the structure of DPB reactor, this paper designed a visual reactor, using salt solution with a mass concentration of 20% as outer electrode, which meant the dielectric was put close to outer electrode, as seen in Figure 2. The discharge region was annular with reaction section length of 65 mm. The inner electrode was stainless steel with an outer diameter of 14 mm and 5 mm separately leading to a discharge gap of 1 mm and 5.5 mm. For the discharge gap of 1 mm, the reactor served as DBD reactor. For the discharge gap of 5.5 mm, filled in with catalyst, the reactor served as DPB reactor. Catalysts used were commercial 40 wt.% Ni/SiO_2, with the column size of Φ2.5 mm × 2.5 mm (Shandong Qilu Keli Chemical Institute Co., Ltd.).

Firstly, the visual reactor was employed to observe normal discharge process. When the voltage regulator supplied a voltage of about 30 V and a current of about 0.5 A, the discharge region began to present random microdischarge with purple light. With the increase of voltage, discharge filaments were gradually thickened and then full of the annular discharge region, as seen in Figure 2.

In DPB reactor, 40 wt.% Ni/SiO_2 catalyst pellets were placed in the discharge region and contacted inner electrode.

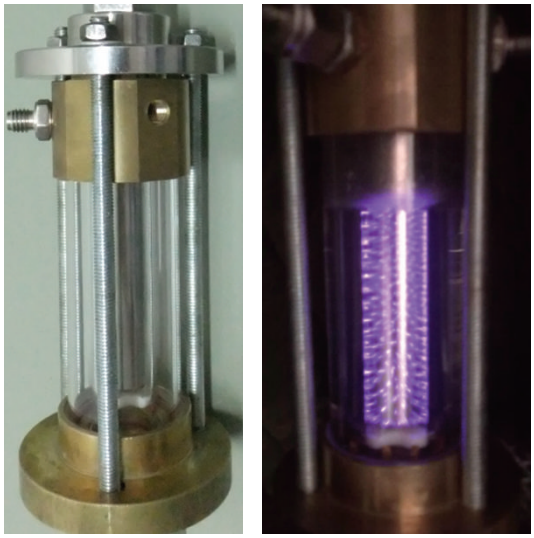

Figure 2: Visual DBD reactor and the discharge phenomenon.

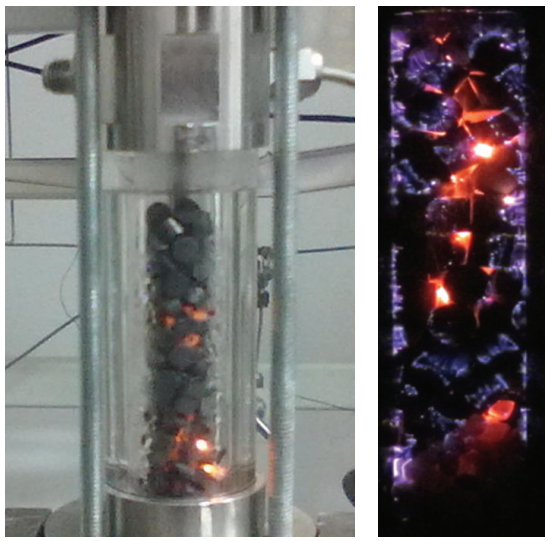

Figure 3: Visual DPB reactor and discharge phenomenon.

After plasma source was on, discharge was nonuniform. The important find was that hot spots (orange light) emerged in the contact area between catalyst and inner electrode, while normal discharge filaments (purple light) still emerged in the contact area between catalyst and dielectric, as shown in Figure 3. The reason might be that 40 wt.% Ni/SiO_2 catalyst pellets became a part of metallic inner electrode, and discharge current flowed through pellet contacts where catalysts were contacted point-to-point, leading to extremely large current density, and then hot spots were produced. However, the hot spots were not expected in DPB reactor, since it would cause a lot of energy consumption. Thus, to avoid hot spots, the structure of reactor was improved by employing double-dielectric structure in the design, as seen in Figure 4, and it was verified that no hot spot appeared.

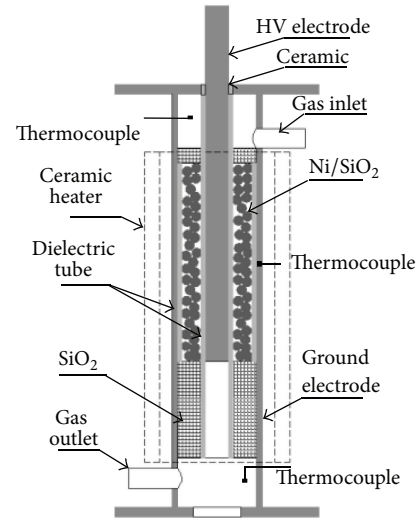

Figure 4: Final DPB reactor.

The performance of reactor was evaluated by methane conversion, products yields, and effective carbon recovery rate. The conversion and yield are defined as follows:

$$\text{Conversion of } CH_4 = \frac{[CH_4]_{\text{inlet}} - [CH_4]_{\text{outlet}}}{[CH_4]_{\text{inlet}}} \times 100, \quad (9)$$

$$\text{Yeild to CO} = \frac{[CO]_{\text{outlet}}}{[CH_4]_{\text{inlet}}} \times 100, \quad (10)$$

$$\text{Yeild to } C_nH_m = \frac{n \times [C_nH_m]_{\text{outlet}}}{[CH_4]_{\text{inlet}}} \times 100, \quad (11)$$

$$\text{Yeild to } H_2 = \frac{[H_2]_{\text{outlet}}}{2 \times [CH_4]_{\text{inlet}}} \times 100. \quad (12)$$

Because of nonequilibrium characteristic of plasma, plasma-assisted methane steam reforming process may produce hydrocarbons C_2, C_3, C_4, and C_5 by type of adiabatic or even exothermic reaction process, which is not conducive to recycling exhaust heat. High hydrocarbons are not conducive to combustion efficiency or the lean-blowout performance of the combustor. Based on these reasons, we propose the concept of effective carbon recovery rate γ to represent the recuperation and combustion characteristics, as seen in

$$\gamma = \frac{[CO]_{\text{outlet}} + [CO_2]_{\text{outlet}} + [CH_4]_{\text{outlet}}}{[CH_4]_{\text{inlet}}}. \quad (13)$$

4.2. Development of Reaction Mechanism. According to the theory of low temperature plasma chemistry, nonequilibrium plasma-assisted reforming process mainly includes electron-impact reactions and free radical reactions. High energy electrons (1 eV < Te < 10 eV) impact CH_4 and H_2O molecules to generate vibrationally excited species, radicals, ions, and electron by excitation, dissociation, and ionization. Radicals generated from electron-impact reactions had predominance

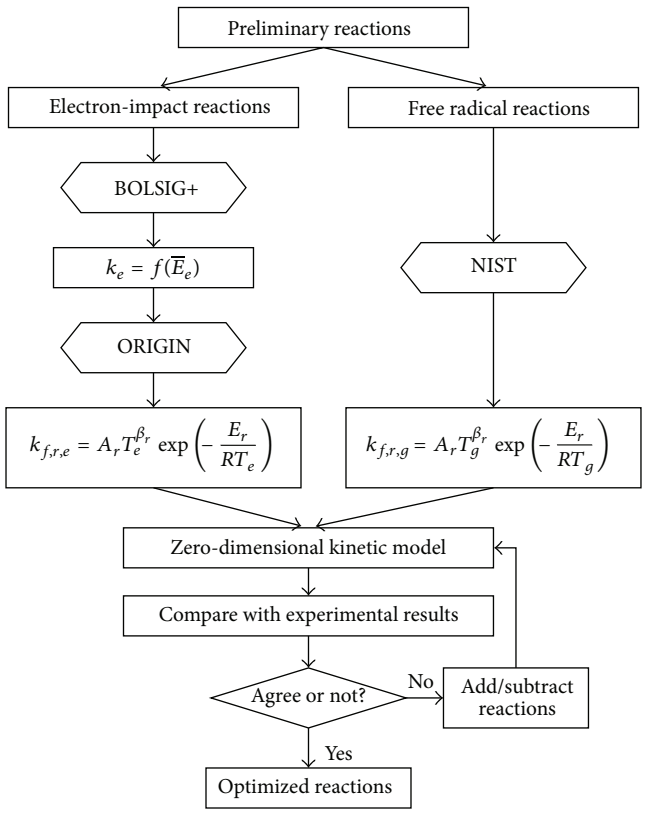

Figure 5: Development diagram of reaction mechanism.

in methane conversion, while ions had little effect on reforming process [15]. According to experimental results, C_2, C_3, C_4, C_5, and C were also included in calculation model. However, in order not to further complicate our plasma reaction mechanism, the higher hydrocarbons (C_4 and C_5) were only treated by two chemical reactions, and some adjustments were made to their Arrhenius coefficients to ensure the agreement between calculation and experimental results.

The effective collisions of electrons in plasma-assisted reforming process occurred only in the group of energetic electrons with a certain probability. This paper took all the electrons with global mean electron energy to substitute for the partial energetic electrons and then established the relationship between rate coefficients of electron-impact reactions and mean electron energy; that is, $k_f = f(\overline{E}_e)$. This dependence was calculated by BOLSIG+ Boltzmann solver [16] based on electron collision cross-section data [17]. Then by means of fitting procedure ORIGIN Arrhenius coefficients of electron-impact reactions were obtained, where electron E was treated just like any other species [14]. The Arrhenius rate coefficients of radical reactions were inquired by NIST Chemistry WebBook [18]. The development diagram of reaction mechanism is shown in Figure 5.

During the development of reaction mechanism, a group of experimental results were chosen as comparison, with the operating conditions of a pressure of 0.12 MPa, reaction temperature of 400°C, total flow of inlet reactants of 7.7×10^{-6} kg/s, S/C of 2, and the input power of 70.13 W. Since the plasma-assisted model was zero-dimensional, it did not solve the Poisson equation for the electric field and therefore did not take into account charge separation and sheath formation near the electrode. Moreover, there were polarization losses as well as ohmic losses in quartz materials. However, it is notable that the research object for kinetic model is gas, not including reactor itself; namely, the input power here totally acts on gas, not on dielectric loss. To distinguish from the input power setting in the experimental operating conditions, a new term "effective input power" for gas in kinetic model was defined. So in the present work, the effective input power P was considered to be an adjustable parameter and varied until methane conversion at reactor outlet was close to experimental results. Once the effective input power was selected, it remained unchanged in the next study to avoid the influence of input power on methane conversion and products yield. At last, the effective input power was selected to fixed value of 56 W and, correspondingly, the calculation conditions used in the model are shown in Table 2.

Table 2: Calculation conditions in the kinetic model for development of reaction mechanism.

Calculation conditions	Values
Gas temperature/K	673
Initial electron temperature/K	11600
Initial molar fraction of reactants	
CH_4	33.333%
H_2O	66.666%
E	0.001%
Pressure/MPa	0.120
Effective input power/W	56
Reactor volume/cm^3	12
Inlet mass flow rate/(kg/s)	7.7×10^{-6}

At last, according to correlative references and experimental results, after correcting and perfecting against the sensitivity analysis module, a total of 175 reactions with 39 species were given out for plasma-assisted MSR (as seen in Appendices A and B in supporting information in the Supplementary Material available online at http://dx.doi.org/10.1155/2014/938618).

Molecular species: E CH_4 H_2O H_2 CO_2 CO C_2H_6 C_2H_4 C_2H_2 CH_3OH CH_3O CH_2O C_3H_8 C_3H_6 C_4H_{10} C_5H_{12}.

Radical species: CH_3 CH_2 CH C C_2H_5 C_2H_3 C_2H HCO OH H O I$*C_3H_7$ N$*C_3H_7$ C_4H_9.

Ionic species: CH_4+ CH_3+ H− CH_2− OH− O− CH_2+ CH+ C+.

4.3. Validation of Plasma-Reforming Kinetic Model. The dependence of methane conversion and products yield on the S/C, reaction temperature, and residence time is shown in Figure 6. In order to validate the plasma-assisted MSR kinetic model, the predicted values in different conditions

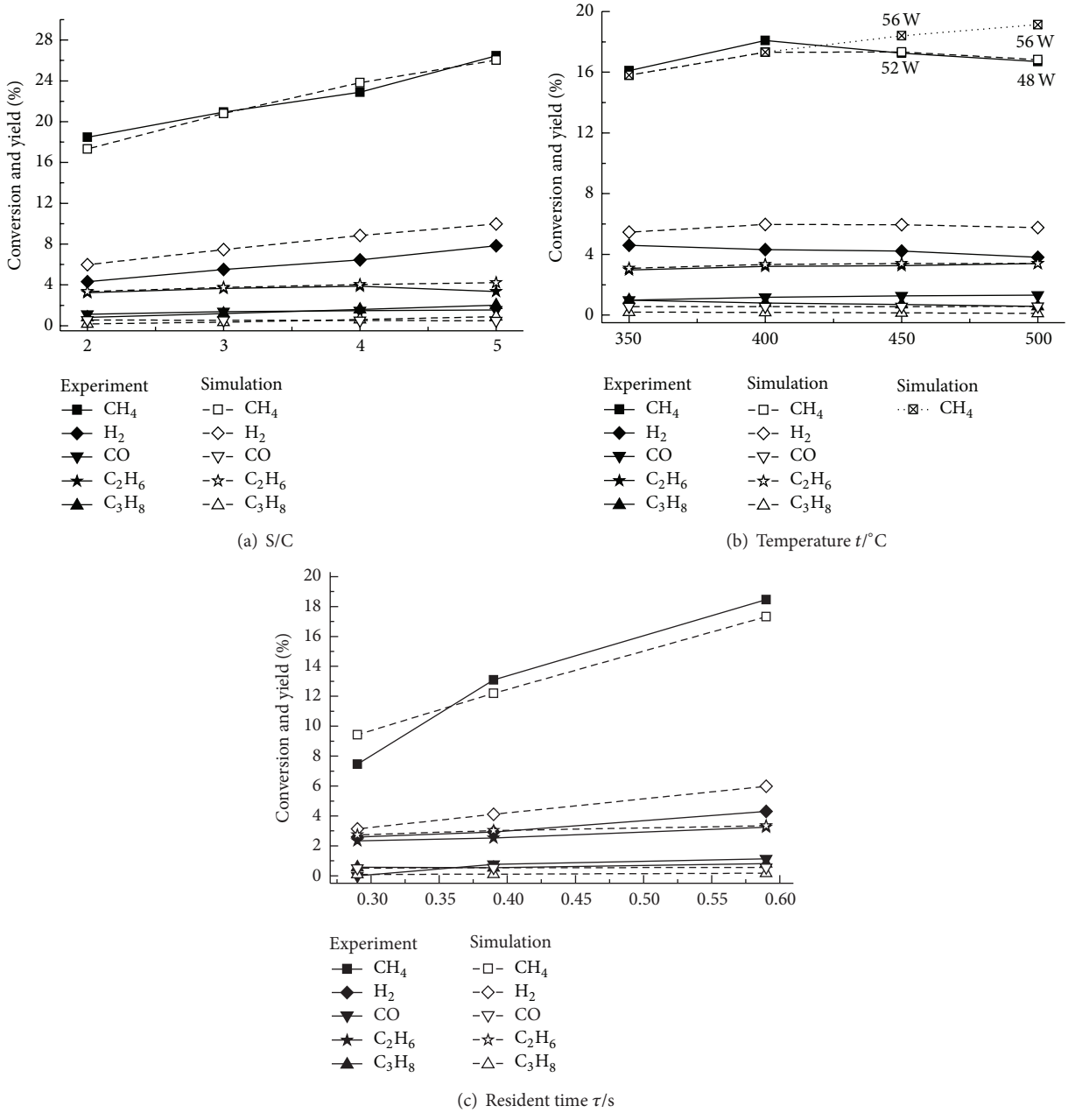

Figure 6: Methane conversion and products yield with increasing S/C (a), reaction temperature (b), and residence time (c).

are also plotted in Figure 6. The model can accurately predict methane conversion and the trend of products yield in different operating conditions, where deviation of C_2H_6 predicted and experimental values is within 4%. But the kinetic model overpredicted H_2 (up to 18%–40%) and underpredicted CO (up to 60%–80%) and C_3H_8 (up to 20%–50%) by volume. During the experiment slightly yellow oil droplets with a pungent odor flowed out with the condensing water, which were higher hydrocarbons liquefied into oil droplets in the cold trap. It proved that part of methane was converted into higher hydrocarbons (C_4 and C_5). However, in the present model, higher hydrocarbons were only treated by two reactions. Thus underestimation of higher hydrocarbons was probably leading to the obvious overestimation of H_2 selectivity in our model. As seen in Figure 8 the dominant formation paths for H_2 were through H abstraction reactions with CH_4, C_2H_6, C_3H_8, $N^*C_3H_7$, and $I^*C_3H_7$, and similar results were reported by Sun et al. [19].

4.4. Kinetic Analysis. As shown in Figure 6(a), with the increase of S/C, CH_4 conversion and yields of H_2 and CO increased. The thing which needed to be firstly declared was that the increase of S/C in the experiment meant that methane content in reactants correspondingly decreased in order to ensure residence time in discharge region constant.

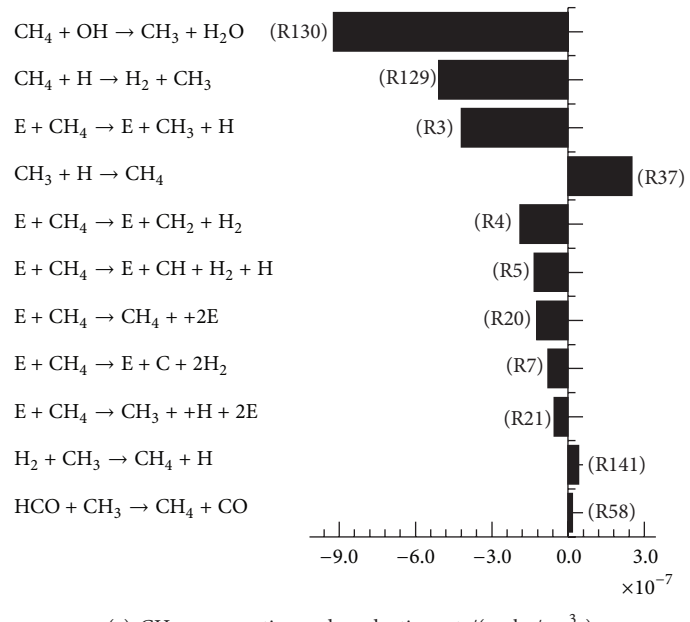

(a) CH_4 consumption and production rate/(moles/cm^{3}s)

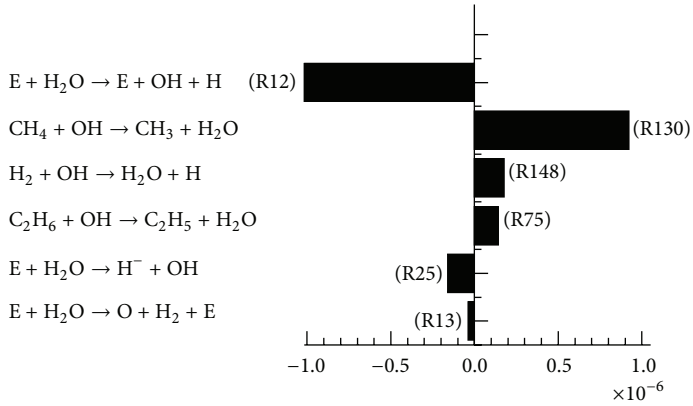

(b) H_2O consumption and production rate/(moles/cm^{3}s)

Figure 7: Calculated time-averaged reaction rates of the dominant reaction pathways for the production and consumption of CH_4 (a) and H_2O (b).

As shown in Figure 7(a), our simulations pointed out that reactions (R130), (R129), (R3), and (R37) were responsible for the production and consumption of CH_4, where OH and H used in reaction (R130) and (R129) were mainly from electron-impact H_2O dissociation reaction (R12), as seen in Figure 7(b). Figure 8(a) shows the effect of S/C on the consumption rate of the above reactions. With increasing S/C, consumption rate of H_2O in reaction (R12) monotonously increased, while consumption rate of CH_4 in reaction (R3) slightly decreased. Although CH_4 content decreased with increasing S/C, consumption rate of CH_4 in reaction (R129) and reaction (R130) remained unchanged due to the increase of OH and H concentration. Figure 8(a) also shows total consumption rate and relative consumption rate of CH_4. Total consumption rate of CH_4 decreased with S/C, which was consistent with the result of Sugasawa et al. [11]. However, due to the decrease of methane content in reactants, the relative consumption rate of CH_4 had a significant increase, resulting in an improvement of methane conversion.

Figure 6(b) shows the influence of reaction temperature on methane conversion and products yield. In numerical simulation, when the effective input power was set in the fixed value of 56 W, methane conversion increased linearly. According to Figure 8(b), temperature had almost no effect on electron-impact dissociation reaction (R3) and (R12), while reaction (R129) was enhanced and total consumption rate of CH_4 increased with temperature increasing. However, experimental results at different reaction temperatures showed that methane conversion presented an increase first and then a decrease with temperature increasing. This might be because polarization losses as well as ohmic losses of quartz materials increased for orders of magnitude due to ionic conductivity when the temperature increased, and thus the power deposition on reactants decreased when input power was constant [20]. So in the numerical study, some adjustments were made for the effective input power, with the value of 56 W into 52 W or 48 W corresponding to reaction temperature of 450°C or 500°C, respectively. After modifying

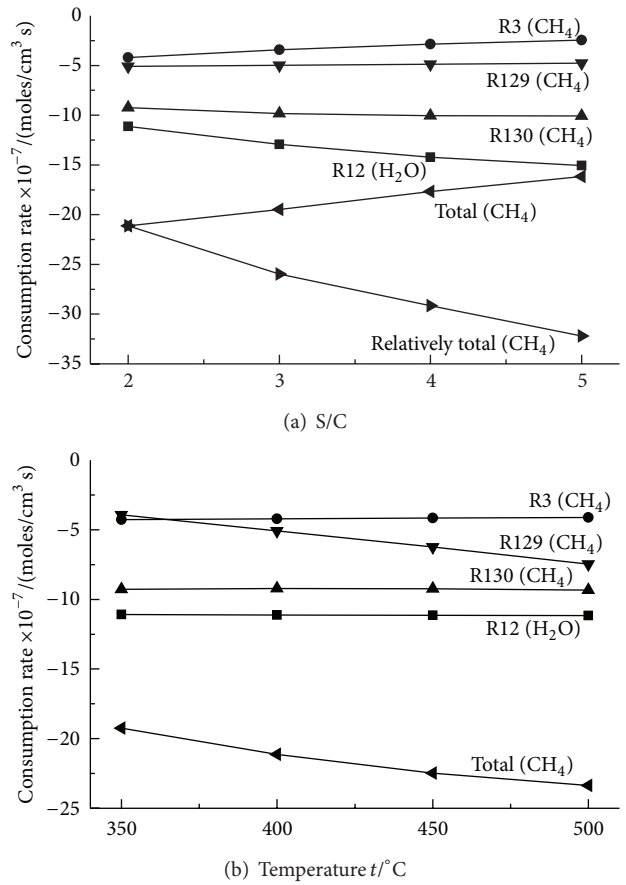

Figure 8: Consumption rate of reactants with increasing S/C (a) and reaction temperature (b).

Table 3: Effect of residence time on product yield.

Product yield/%	Residence time τ/s		
	0.29	0.39	0.58
C_4H_{10}	4.610	6.584	10.553
C_5H_{12}	0.004	0.006	0.009

the effective input power accordingly, methane conversion in simulation was in good agreement with the experimental values, that is, the dash line in Figure 6(b), which also implied and proved the effect of temperature on property of quartz materials.

Figure 6(c) shows that methane conversion and products yield significantly increased with an increase of residence time. Since the effective input power was constant, the number of energetic electron and electron energy remained unchanged. The longer the residence time was, the higher the probability of electron-impact CH_4 was, which resulted in more chance for CH_4 molecule to be activated. Moreover, as the residence time increased, C_2 and C_3 generated were further dehydrogenated to couple, which is another reason for the improvement of methane conversion. The yield of higher hydrocarbons under different residence time s is shown in Table 3.

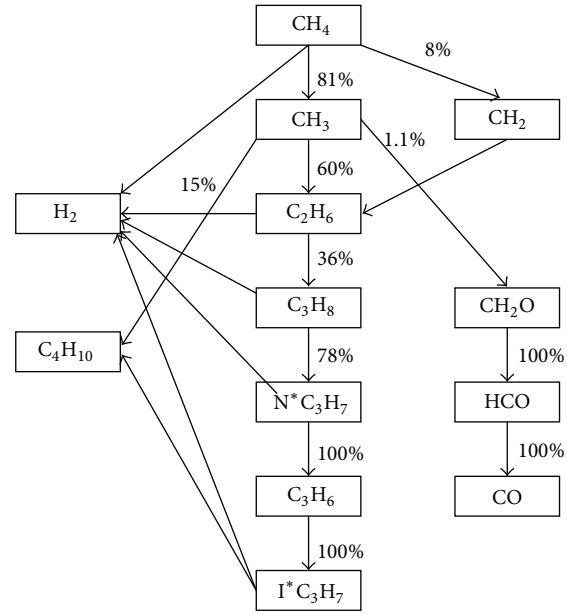

Figure 9: Reaction path flux analysis.

4.5. Reaction Path Flux Analysis. In order to identify the reactions which could affect the selectivity of products in plasma-assisted methane steam reforming process, path flux analysis was performed in the condition of a pressure of 0.12 MPa, reaction temperature of 400°C, total flow of inlet reactants of 7.7×10^{-6} kg/s, S/C of 2, and input power of 70.13 W, as shown in Figure 9. CH_3 was dissociated from methane mainly by H abstraction with OH and H produced via plasma discharge. Methane was also decomposed into CH_3 and CH_2 via electron collisions. Known from experimental results, CO yield was low, only 1%, and light hydrocarbons (C_2 and C_3) yield was at around 4%. This can be explained by Figure 9. It shows that 60% CH_3 were recombined into C_2H_6 and furthermore into higher hydrocarbons by dehydrogenation coupling, while only 1.1% CH_3 was combined with O and through a series of reaction pathways $CH_3 + O \rightarrow CH_2O \rightarrow HCO \rightarrow CO$ finally converted into CO.

According to (14) and (15), the reaction of methane converted to synthesis gas was strongly endothermic reaction, and the coupling reaction of methane converted to hydrocarbons was weakly endothermic reaction which was not beneficial for waste heat recovery. Therefore increasing synthesis gas yield and decreasing higher hydrocarbon yield were the main means of improving heat recovery. According to the path analysis diagram, there should mainly be two measures: (1) inhibit CH_3 from recombining into C_2H_6; (2) improve O radical concentration, namely, improve reaction rate of CH_3 and O combination. Figure 7(b) points out that reaction (R12) was responsible for 83% of the total electron-impact dissociation of H_2O, while reaction (R13) was responsible for 3%, which was to say OH concentration was higher than O concentration. Badly most of OH was combined with CH_4 to regenerate H_2O. Therefore, inhibiting the combination of OH

Table 4: Comparisons of methane steam reforming in different reactors.

Reforming results	DBD reactor	DPB reactor
Effective carbon recovery rate/%	87.44	100.00
Methane conversion/%	13.10	11.43
Product yield/%		
H_2	2.93	45.83
CO	0.54	0.18
CO_2	0.00	10.89
C_2H_6	2.53	0.00
C_3H_8	0.76	0.00

and CH_4 and promoting the transformation from OH into O were the key to improve O radical concentration.

Known from surface reaction mechanism of MSR over Ni, as seen in (16)–(23) [21], choosing a suitable catalyst can guarantee free radicals produced by electron-impact reactions to adsorb onto the surface of catalysts. The selectivity characteristics of catalysts can effectively lower the recombination of alkyl and improve OH into O, which can improve the yield of synthesis gas:

$$CH_4 + H_2O \longrightarrow CO + 3H_2 \quad Q = -206\,\text{kJ/mol} \tag{14}$$

$$CH_4 + CH_4 \longrightarrow C_2H_6 + H_2 \quad Q = -66\,\text{kJ/mol} \tag{15}$$

$$NI\,(s) + CH_3\,(s) \longrightarrow H\,(s) + CH_2\,(s) \tag{16}$$

$$NI\,(s) + CH_2\,(s) \longrightarrow H\,(s) + CH\,(s) \tag{17}$$

$$NI\,(s) + CH\,(s) \longrightarrow H\,(s) + C\,(s) \tag{18}$$

$$NI\,(s) + OH\,(s) \longrightarrow H\,(s) + O\,(s) \tag{19}$$

$$OH\,(s) + CH_3\,(s) \longrightarrow CH_4\,(s) + O\,(s) \tag{20}$$

$$OH\,(s) + CH_2\,(s) \longrightarrow CH_3\,(s) + O\,(s) \tag{21}$$

$$OH\,(s) + CH\,(s) \longrightarrow CH_2\,(s) + O\,(s) \tag{22}$$

$$OH\,(s) + C\,(s) \longrightarrow CH\,(s) + O\,(s)\,. \tag{23}$$

To preliminarily verify the reaction path flux analysis, plasma catalytic hybrid reforming experiment was employed in DPB reactor. The operating conditions were pressure of 0.12 MPa, reaction temperature of 400°C, total flow of inlet reactants of 1.156×10^{-5} kg/s, S/C of 2, and the input power of 70.13 W. The characteristics for steam reforming are shown in Table 4. After adding Ni catalyst on discharge region, synthesis gas yield had a significant improvement, $C_2 + C_3$ yield was equal to zero, and no higher hydrocarbons were produced, with an effective carbon recovery rate of 100%. Those results verified the reaction path flux analysis, which also indirectly proved the validity of reaction mechanism for plasma-assisted MSR developed in this paper.

5. Conclusions

In this paper we designed a visual reactor and confirmed a double-dielectric structure for DPB reactor. Experimental studies of plasma-assisted MSR were performed at different S/C, residence time s, and reaction temperatures. Based on the experimental results, a detailed reaction mechanism for plasma-assisted MSR was built and developed. The results are summarized as follows.

(1) DBD assisted methane steam reforming technology can improve methane conversion in low temperature without catalyst but cause a low effective carbon recovery rate. In different operating conditions, CO yield is only around 1%, lower hydrocarbons (C_2, C_3) yield is about 4%, and the residual of reacting CH_4 is converted into higher hydrocarbons (more than C_4).

(2) The kinetic model developed can accurately predict methane conversion and the trend of products yield in different operating conditions. The reactions of $CH_3 + CH_3 \rightarrow C_2H_6$ and $OH + CH_4 \rightarrow H_2O + CH_3$ act as limiting reactions for CO yield.

(3) Adding Ni catalyst in discharge region can guarantee free radicals to adsorb onto the catalyst surface and thus improve yields of syngas and avoid generation of higher hydrocarbons.

Nomenclature

Variable Physical Dentitions

ρ: Mass density (kg/m^3)
V: Reactor volume (m^3)
$\dot{m}^*$: Inlet mass flow rate (kg/s)
$\dot{m}$: Outlet mass flow rate (kg/s)
Y_k: The mass fraction of the kth species
W_k: Molecular weight of the kth species
$\dot{\omega}_k$: Molar rate of production of the kth species (mol/m^3·s)
p: Mixture pressure (MPa)
T_g: Gas temperature (K)
T_e: Electron temperature (K)
ν_{ek}: Momentum-transfer collision frequency
I_{er}: Total number of electron-impact reactions
q_r: Net rate of progress of the rth reaction
ΔH_r: Net enthalpy change of the reaction
X_k: Molar concentration of the kth species
$k_{f,r}$: Forward rate constants of the rth reaction
$k_{b,r}$: Reverse rate constants of the rth reaction
v'_{kr}: Stoichiometric coefficient for reactant k in reaction r
v''_{kr}: Stoichiometric coefficient for product k in reaction r
A_r: Preexponential factor
β_r: Temperature exponent
E_r: Activation energy
$\overline{E}_e$: Mean electron energy
Bracket []: Molar concentration of species.

Subscript

k: Specific species
r: Specific reaction
e: Electron
g: Gas.

Superscript

*: Inlet stream quantities.

Conflict of Interests

The authors declare that there is no conflict of interests regarding the publication of this paper.

Acknowledgments

The authors wish to thank Mr. Long Qiang and Mr. Xu Changsong for their assistance in constructing the test rig and also appreciate the authors of the following references.

References

[1] I. Rusu and J.-M. Cormier, "On a possible mechanism of the methane steam reforming in a gliding arc reactor," *Chemical Engineering Journal*, vol. 91, no. 1, pp. 23–31, 2003.

[2] D. Petrovi, T. Martens, J. V. Dijk, W. J. M. Brok, and A. Bogaerts, "Modeling of a dielectric barrier discharge used as a flowing chemical reactor," *Journal of Physics: Conference Series*, vol. 133, no. 1, pp. 1–8, 2008.

[3] S. A. Nair, T. Nozaki, and K. Okazaki, "Methane oxidative conversion pathways in a dielectric barrier discharge reactor—investigation of gas phase mechanism," *Chemical Engineering Journal*, vol. 132, no. 1–3, pp. 85–95, 2007.

[4] J. Li, Y.-J. Wang, H.-L. Long, Y.-X. Yin, and X.-Y. Dai, "Townsend ionization model and kinetic analysis of methane activated in strong electric field," *Chemical Engineering*, vol. 35, no. 8, pp. 25–28, 2007 (Chinese).

[5] C. de Bie, T. Martens, J. Van Dijk et al., "Dielectric barrier discharges used for the conversion of greenhouse gases: modeling the plasma chemistry by fluid simulations," *Plasma Sources Science and Technology*, vol. 20, no. 2, Article ID 024008, pp. 1–11, 2011.

[6] Y.-F. Wang, C.-H. Tsai, W.-Y. Chang, and Y.-M. Kuo, "Methane steam reforming for producing hydrogen in an atmospheric-pressure microwave plasma reactor," *International Journal of Hydrogen Energy*, vol. 35, no. 1, pp. 135–140, 2010.

[7] T. Nozaki, N. Muto, S. Kadio, and K. Okazaki, "Dissociation of vibrationally excited methane on Ni catalyst: part 2. Process diagnostics by emission spectroscopy," *Catalysis Today*, vol. 89, no. 1-2, pp. 67–74, 2004.

[8] H. Kabashima, H. Einaga, and S. Futamura, "Hydrogen generation from water, methane, and methanol with nonthermal plasma," *IEEE Transactions on Industry Applications*, vol. 39, no. 2, pp. 340–345, 2003.

[9] S. Futamura and G. Annadurai, "Plasma reforming of aliphatic hydrocarbons with CO_2," *IEEE Transactions on Industry Applications*, vol. 41, no. 6, pp. 1515–1521, 2005.

[10] L. A. Rosocha, Y. Kim, G. K. Anderson, S. Abbate, and R. Sanchez-Gonzalez, "Non-thermal plasma-assisted combustion research at los alamos," in *Proceedings of the 16th IEEE International Pulsed Power Conference*, vol. 2, pp. 1391–1394, Albuquerque, NM, USA, June 2007.

[11] M. Sugasawa, T. Terasawa, and S. Futamura, "Effects of initial water content on steam reforming of aliphatic hydrocarbons with nonthermal plasma," *Journal of Electrostatics*, vol. 68, no. 3, pp. 212–217, 2010.

[12] D. H. Lee, K.-T. Kim, M. S. Cha, and Y.-H. Song, "Plasma-controlled chemistry in plasma reforming of methane," *International Journal of Hydrogen Energy*, vol. 35, no. 20, pp. 10967–10976, 2010.

[13] X. Zhang, B. W. Wang, Y. W. Liu, and G. H. Xu, "Conversion of methane by steam reforming using dielectric-barrier discharge," *Chinese Journal of Chemical Engineering*, vol. 17, no. 4, pp. 625–629, 2009.

[14] R. J. Kee, F. M. Rupley, E. Meeks, and J. A. Miller, "Chemkin-III: a Fortran chemical kinetics package for the analysis of gas-phase chemical and plasma kinetic," CHEMKIN-PRO SAND96-8216.1996, Reaction Design, San Diego, Calif, USA, 2008.

[15] K. Hiraoka, K. Aoyama, and K. Morise, "A study of reaction mechanisms of methane in a radio-frequency glow discharge plasma using radical and ion scavengers," *Canadian Journal of Chemistry*, vol. 63, no. 11, pp. 2899–2905, 1985.

[16] PHELPS database, 2012, http://www.lxcat.laplace.univ-tlse.fr.

[17] G. J. M. Hagelaar and L. C. Pitchford, "Solving the Boltzmann equation to obtain electron transport coefficients and rate coefficients for fluid models," *Plasma Sources Science and Technology*, vol. 14, no. 4, pp. 722–733, 2005.

[18] 2012, http://webbook.nist.gov/chemistry/form-ser.html.

[19] W. T. Sun, M. Uddi, S. H. Won, T. Ombrello, C. Carter, and Y. Ju, "Kinetic effects of non-equilibrium plasma-assisted methane oxidation on diffusion flame extinction limits," *Combustion and Flame*, vol. 159, no. 1, pp. 221–229, 2012.

[20] T. Hammer, T. Kappes, and M. Baldauf, "Plasma catalytic hybrid processes: gas discharge initiation and plasma activation of catalytic processes," *Catalysis Today*, vol. 89, no. 1-2, pp. 5–14, 2004.

[21] V. M. Janardhanan and O. Deutschmann, "CFD analysis of a solid oxide fuel cell with internal reforming: coupled interactions of transport, heterogeneous catalysis and electrochemical processes," *Journal of Power Sources*, vol. 162, no. 2, pp. 1192–1202, 2006.

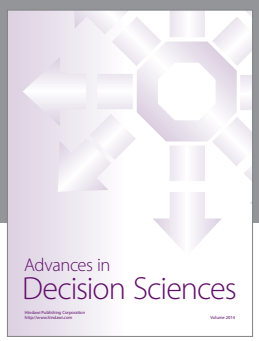

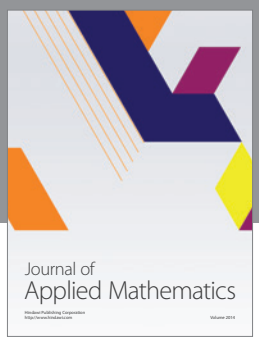

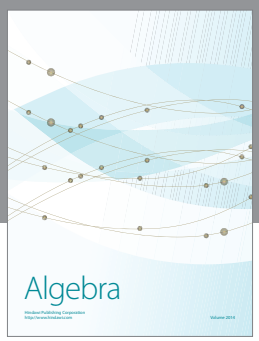

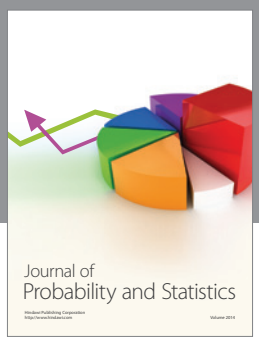

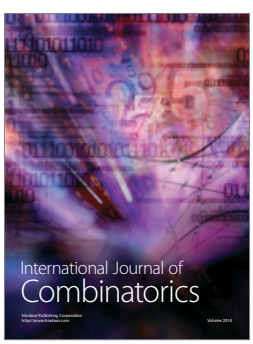

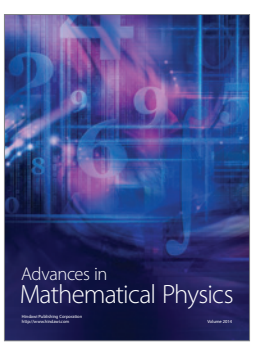

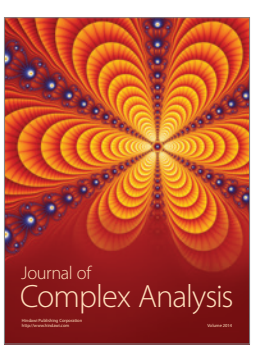

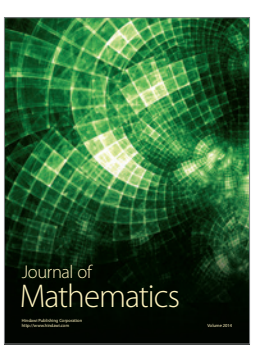

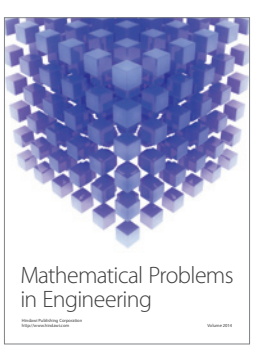

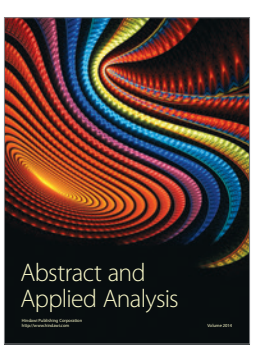

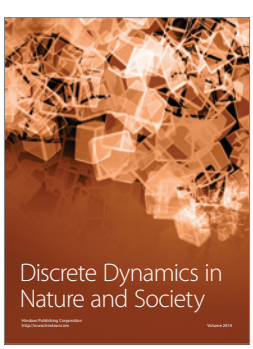

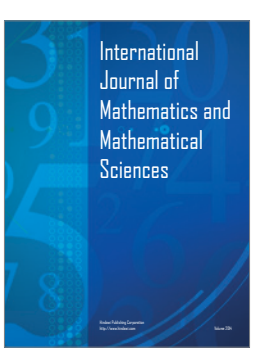

Hindawi

Submit your manuscripts at
http://www.hindawi.com